

Film Thermoelectric Generator of Multiple Two-Dimensional Electron Gas

Yuto Uematsu, Takafumi Ishibe, Seiya Kozuki, Takaaki Mano, Akihiro Ohtake, Hideki T. Miyazaki, Takeshi Kasaya, Yuichiro Yamashita, Mutsunori Uenuma, and Yoshiaki Nakamura

Abstract—Two-dimensional electron gas (2DEG) is one of the promising approaches for high thermoelectric performance. However, high electrical resistance of the film originating from thin 2DEG conduction channel width and thick insulator layer is a bottleneck for obtaining high output power. In this study, we propose stacked GaAs 2DEG thermoelectric generator (TEG), which has a number of stacked channel structures for low electrical resistance. Our GaAs 2DEG TEGs with channels formed in triangular well exhibit ultrahigh thermoelectric power factor. In addition, the interfaces of the stacked 2DEG intensify phonon scatterings, resulting in the reduction of thermal conductivity. The stacked 2DEG TEGs exhibit 9 times higher sheet electrical conductivity than the unstacked 2DEG one, resulting in ~ 7.5 times higher output power of stacked 2DEG TEGs (5.1 nW) than that of unstacked 2DEG ones. Cross-sectional thermoelectric efficiency factor of stacked 2DEG TEGs reaches $3.7 \mu\text{W cm}^{-2}\text{K}^{-2}$. This value is the highest among various simple planar type film TEGs without cavities under the film. This TEG demonstration will open an avenue for the social application of 2DEG TEG.

Index Terms—Energy harvesting, thermoelectric materials, thermoelectric devices, two-dimensional electron gas.

I. Introduction

FILM thermoelectric generator (TEG), which directly converts heat to electricity, has drawn much attention as one of the sustainable energy power sources for running internet of things sensors [1], [2]. Toward various application places, there have been a lot of studies about film TEGs on various substrates, such as processable Si, flexible polyimide, and transparent $\text{r-Al}_2\text{O}_3$ [3]–[7]. To enhance the performance of film TEG, it is essential to optimize the TEG structure and enhance the performance of the thermoelectric (TE) materials [8], [9].

The TE performance is strongly related to a dimensionless

Manuscript received xxxxx, x, xxxx. This work was supported by Grant-in-Aid for Scientific Research A (Grant No. 23H00258), JSPS Fellows (T22KJ2052), and "Advanced Research Infrastructure for Materials and Nanotechnology in Japan (ARIM)" of the Ministry of Education, Culture, Sports, Science and Technology (MEXT) (JPMXP1223NM5062). (Corresponding author: Yoshiaki Nakamura.)

Y. Uematsu, T. Ishibe, S. Kozuki, and Y. Nakamura are with the Graduate School of Engineering Science, Osaka University, Osaka 560-8531, Japan (e-mail: nakamura.yoshiaki.es@osaka-u.ac.jp).

T. Mano, A. Ohtake, H. T. Miyazaki, and T. Kasaya are with the National Institute for Materials Science, Ibaraki 305-0047, Japan.

Y. Yamashita is with the National Institute of Advanced Industrial Science and Technology, Ibaraki 305-8565, Japan.

M. Uenuma is with the National Institute of Advanced Industrial Science and Technology, Saga 841-0052, Japan.

figure of merit zT ; $zT = S^2 \sigma T \kappa^{-1}$, where S is Seebeck coefficient, σ is electrical conductivity, κ is thermal conductivity, and T is absolute temperature. The central issue for high zT is the independent control of the intercorrelated TE three parameters. Nanostructuring approach has reduced κ drastically, leading to high zT [10]–[16]. On the other hand, as for $S^2 \sigma$ enhancement [17]–[22], quantum confinement effect is well-known as one of the promising approaches [23]–[25]. For example, some groups have reported remarkable $S^2 \sigma$ enhancements using two-dimensional electron gas (2DEG) [26], [27]. In 2024, we proposed the multiplied 2DEG effect that S of multiple 2DEG (M-2DEG), where multiple subbands in triangular quantum well contribute to electrical conduction, is higher than that of single 2DEG (S-2DEG) with a single subband (Fig. 1(a)) [28]. This S enhancement is also confirmed even when we plot S as a function of sheet carrier concentration n_s (Fig. 1(b)). This result implies that S enhancement by multiplied 2DEG effect [28] does not depend on the definition of the channel width of 2DEG. This effect brought the drastic enhancement of $S^2 \sigma$, which is beyond the theoretical prediction of $S^2 \sigma$ in the conventional 2DEG (Hicks and Dresselhaus theory [23]). This makes us expect that the TEG using M-2DEG can exhibit high output power P_{out} . However, high electrical resistance R of the film originating from thin channel width of 2DEG and thick insulator layer is a bottleneck for high P_{out} .

In this study, we propose the planar unileg-type stacked GaAs 2DEG TEG composed of M-2DEG film, which has stacked channel structures for low R , namely large cross-sectional area of electrical conduction layer (Fig. 1(c)). Our GaAs 2DEG TEGs with channels formed in triangular well exhibited ultrahigh $S^2 \sigma$ because of multiplied 2DEG effect. In addition, the out-of-plane κ of the stacked GaAs 2DEG TEGs was ~ 3 times lower than that of GaAs bulk because of the intensified interface phonon scattering. This leads to the increase of T difference ΔT between hot and cold side. The stacked 2DEG TEGs exhibited 9 times higher sheet electrical conductivity than the unstacked 2DEG TEGs with only one 2DEG channel, resulting in higher P_{out} of stacked 2DEG TEGs than that of unstacked 2DEG TEGs. We evaluated the TE efficiency factor ϕ ; $\phi = P_{\text{max}} / (A \times \Delta T^2)$, where P_{max} is the maximum value of P_{out} , A is the area of the TEG. The ϕ calculated using the total cross-sectional area of the TE legs of the planar unileg-type stacked GaAs 2DEG film TEGs reached $3.7 \mu\text{W cm}^{-2}\text{K}^{-2}$, which was the highest among various simple planar type film TEGs without cavities under the film. This

study highlights that stacked GaAs 2DEG TEGs become a promising TEG.

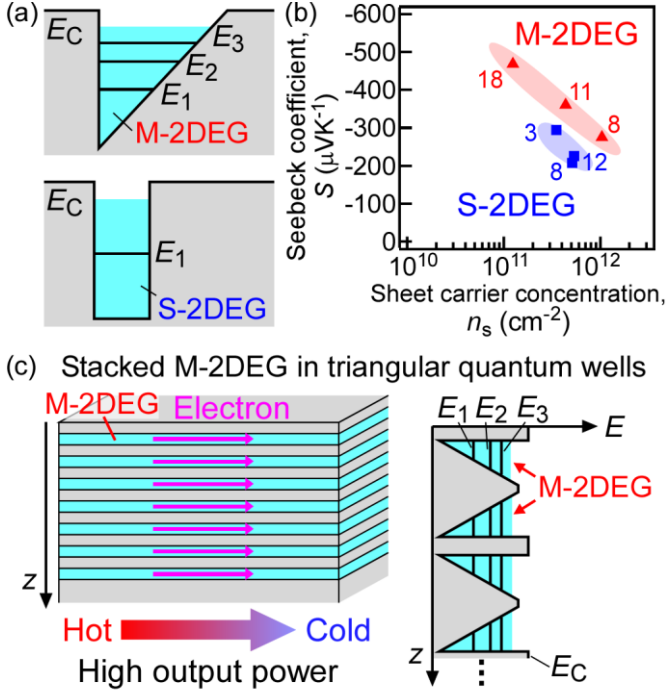


Fig. 1. (a) The schematic illustrations of M-2DEG in triangular quantum well and S-2DEG in rectangular quantum well. (b) S - n_s plot of M-2DEG and S-2DEG. The numbers around the experimental data points represent the channel width of 2DEG. (c) The schematic illustration of stacked 2DEG with triangular quantum wells and its energy band diagram.

II. EXPERIMENTAL

A. Formation of GaAs 2DEG Films

Figure 2(a) shows the structures of stacked M-2DEG films (9 times stacked 2DEG channels) and unstacked M-2DEG films. These samples were epitaxially grown on GaAs(001) substrates using molecular beam epitaxy in the following processes. To obtain clean surfaces of undoped GaAs(001) substrates, undoped GaAs (300 nm) initial layers were formed on the GaAs substrates. Subsequently, as the buffer layers, GaAs/ $\text{Al}_{0.3}\text{Ga}_{0.7}\text{As}$ superlattice layers were formed on the undoped GaAs/GaAs substrates by alternately depositing GaAs (10 nm) and $\text{Al}_{0.3}\text{Ga}_{0.7}\text{As}$ (10 nm) 20 times. In the case of stacked 2DEG films, the unit structure of undoped $\text{Al}_{0.3}\text{Ga}_{0.7}\text{As}$ (2 nm)/ undoped GaAs (150 nm)/ undoped $\text{Al}_{0.3}\text{Ga}_{0.7}\text{As}$ (2 nm)/ Si-doped $\text{Al}_{0.3}\text{Ga}_{0.7}\text{As}$ (40 nm, dopant concentration: $7 \times 10^{17} \text{ cm}^{-3}$) layers was formed 4 times repeatedly on the buffer layers. Finally, stacked layers of undoped $\text{Al}_{0.3}\text{Ga}_{0.7}\text{As}$ (2 nm)/ undoped GaAs (150 nm)/ undoped $\text{Al}_{0.3}\text{Ga}_{0.7}\text{As}$ (2 nm)/ Si-doped $\text{Al}_{0.3}\text{Ga}_{0.7}\text{As}$ (60 nm, dopant concentration: $7 \times 10^{17} \text{ cm}^{-3}$) and GaAs (10 nm) cap layers were formed. 2DEG channels were formed at the AlGaAs/GaAs interfaces of the top and bottom of 150 nm undoped GaAs layers except for the first undoped GaAs layer just above the buffer layer. In the case of unstacked 2DEG films, the structure of undoped $\text{Al}_{0.3}\text{Ga}_{0.7}\text{As}$ (2 nm)/ undoped GaAs (100 nm)/ undoped $\text{Al}_{0.3}\text{Ga}_{0.7}\text{As}$ (2 nm)/ Si-doped $\text{Al}_{0.3}\text{Ga}_{0.7}\text{As}$ (80 nm, dopant concentration: $7 \times 10^{17} \text{ cm}^{-3}$)

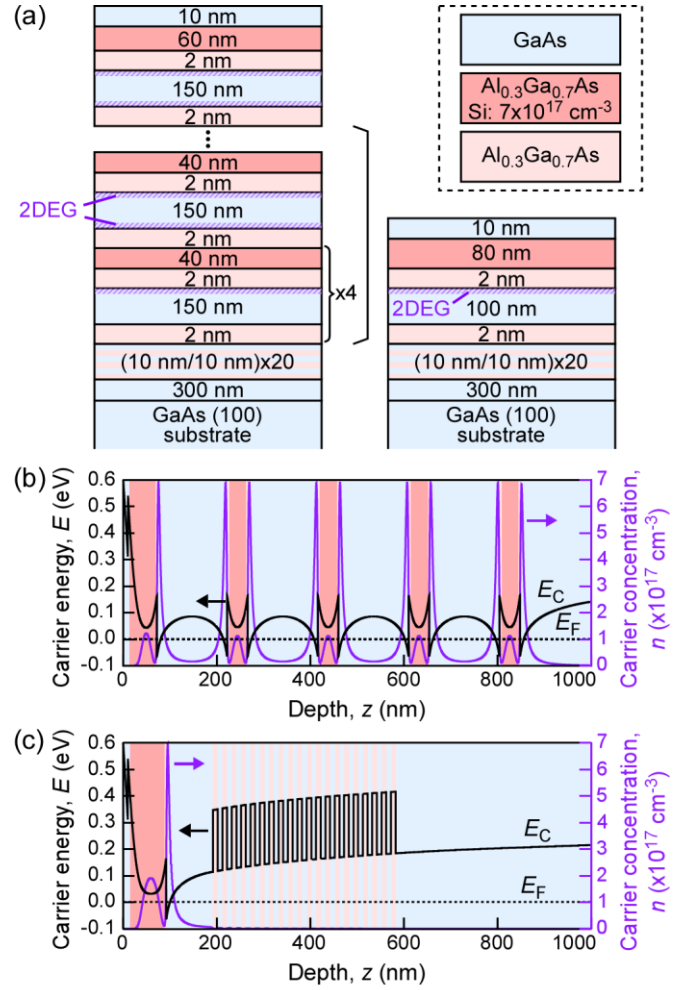


Fig. 2. (a) Structures of stacked 2DEG film and unstacked 2DEG film on the buffer layers of GaAs (10nm) / $\text{Al}_{0.3}\text{Ga}_{0.7}\text{As}$ (10 nm) \times 20 times on GaAs (300 nm) on GaAs(100) substrate. (b) Energy band structures of stacked 2DEG film and (c) unstacked 2DEG film.

cm^{-3}) layers was formed once on buffer layers. Finally, GaAs (10 nm) cap layer was formed. In the epitaxial growth, two kinds of growth temperatures were used: 823 and 853 K. To suppress the diffusion of Si (ionized impurity) into the 2DEG channel, we formed the following two layers at low T of 823 K: (1) the Si-doped $\text{Al}_{0.3}\text{Ga}_{0.7}\text{As}$ layers and (2) the 2 nm undoped $\text{Al}_{0.3}\text{Ga}_{0.7}\text{As}$ layers on the Si-doped $\text{Al}_{0.3}\text{Ga}_{0.7}\text{As}$ ones. On the other hand, the other layers were formed at high T of 853 K to enhance the crystallinity.

The energy band diagrams and the carrier concentrations (n) along the depth (z) direction were calculated using Schrödinger-Poisson equation self-consistently computed by 1D Poisson [29], as shown in Figs. 2(b) and (c). It was clearly found that 2DEG channels were formed at the interfaces of AlGaAs/GaAs by modulation doping. A width of the 2DEG channel was defined as 8 nm by the full width at half maximum of z - n profiles, the definition of which is widely used in the previous studies [24], [28]. Therefore, the total thickness of 2DEG layers ($t_{2\text{DEG}}$) in stacked 2DEG and unstacked 2DEG films were simply estimated to be 72 nm ($8 \text{ nm} \times 9$ channels) and 8 nm, respectively.

B. Fabrication of GaAs 2DEG TEGs

The fabrication processes of the planar unileg-type stacked GaAs 2DEG film TEG are shown in Figs. 3(a)-(d). TE legs of stacked 2DEG film were formed by wet etching with the mixed solution of H_3PO_4 (85 wt%, 2 mL), H_2O_2 (35 wt%, 2 mL), and H_2O (16 mL). Then, the inclined facets at the sides of stacked 2DEG TE legs appeared (Fig. 3(e)), and the AlGaAs/GaAs interfaces with 2DEG channels were bared. These bared structures enable us to easily make ohmic contact with all the 2DEG channels (Fig. 3(f)). To make ohmic contact with 2DEG channels, the stacked metal electrodes of Ni (5 nm)/AuGe (50 nm)/Ni (30 nm)/Au (100 nm) were deposited on the both ends of TE legs, and were annealed for 90 seconds at 450°C . These isolated TE legs with ohmic electrodes were serially connected with wire electrodes of Ti (30 nm)/Au (400 nm).

The plan-view photograph of the fabricated stacked 2DEG TEG and its schematic illustration are shown in Figs. 3(g) and (h), respectively. The size of the TE legs: length L_{tl} \times width W_{tl} \times thickness t_{tl} in unstacked (stacked 2DEG TEG) is $4\text{ mm} \times 500\text{ }\mu\text{m} \times 0.19\text{ }\mu\text{m}$ ($4\text{ mm} \times 500$ or $200\text{ }\mu\text{m} \times 1\text{ }\mu\text{m}$). The numbers of TE legs n_{tl} of the TEGs with $W_{\text{tl}} = 500\text{ }\mu\text{m}$ and with $W_{\text{tl}} = 200\text{ }\mu\text{m}$ are 12 and 21, respectively. The size of the Ti/Au wire

electrodes (length $L_w \times$ width $W_w \times$ thickness t_w) is $4\text{ mm} \times 100\text{ }\mu\text{m} \times 0.43\text{ }\mu\text{m}$. The size of Ti/Au wire (length $L_{w2} \times$ width $W_{w2} \times$ thickness t_{w2}) between the TE leg and the wire electrode is $50\text{ }\mu\text{m} \times 300\text{ }\mu\text{m} \times 0.43\text{ }\mu\text{m}$.

C. Measurement Method of TE Properties

Sheet electrical conductivity σ_s , n_s , and carrier mobility μ of the unstacked 2DEG and the stacked 2DEG films were measured using van der Pauw method and Hall effect measurement along in-plane direction. σ and n were obtained by dividing the measured σ_s and n_s by $t_{2\text{DEG}}$. S was measured using ZEM-3 (ADVANCE RIKO Inc.). κ along the out-of-plane direction was measured using time domain thermoreflectance (TDTR) method. During the measurement of the output voltages V_{out} , the output current I_{out} , and the P_{out} of GaAs 2DEG TEGs at room temperature, ΔT was applied by Peltier heater. T distribution in the GaAs 2DEG TEG was measured using InfraScope MWIR temperature mapping microscope (Quantum Focus Instruments Co.).

III. RESULTS AND DISCUSSION

A. TE Properties of GaAs 2DEG Films

T dependences of TE properties of unstacked and stacked 2DEG films were measured (Fig. 4). When estimating n and σ of 2DEG films, we used the following $t_{2\text{DEG}}$: 72 nm (8 nm \times 9 channels) for stacked 2DEG films; 8 nm for unstacked 2DEG films. Comparing the TE properties of unstacked and stacked 2DEG films in the measurement T range, there were almost no differences in n , μ , σ , and S (Figs. 4(a)-(d)). Therefore, both unstacked and stacked 2DEG films exhibited almost the same $S^2\sigma$ in the measurement T range (Fig. 4(e)). We discuss the tendencies of the TE properties against T . As shown in Fig. 4(a), both 2DEG films showed almost no T dependences of n . Figures 4(b) and (c) are T dependences of μ and σ , respectively. μ values of unstacked and stacked 2DEG films drastically decreased with increasing T . The strong T dependences of μ and the extremely high μ values are consistent with the results reported by previous studies about modulation doped 2DEG [28], [30]. This indicates that in both 2DEG films, carriers travel in 2DEG channels without ionized impurity. Because of strong T dependences of μ , unstacked and stacked 2DEG films also showed strong T dependences of σ (Fig. 4(c)). On the other hand, S values of unstacked 2DEG and stacked 2DEG films increased monotonically with increasing T . This is conventional tendency, which is because the average energy per unit conducting electron increased with T increase (Fig. 4(d)).

The correspondence between the TE properties of unstacked and stacked 2DEG films demonstrates that TE properties of all the 2DEG channels in stacked 2DEG film are the same as that in unstacked 2DEG film. This indicates that stacked 2DEG films have almost nine times larger σ_s than unstacked 2DEG films, as shown in Fig. 4(f). σ_s is almost proportional to the number of channels. Therefore, it is expected that stacked 2DEG TEG exhibits higher P_{out} than unstacked 2DEG films because of the lower R .

The out-of-plane thermal conductivity, κ_0 of the stacked 2DEG film was measured to be $15.9 \pm 0.4\text{ Wm}^{-1}\text{K}^{-1}$, which is ~ 3 times smaller than κ of GaAs bulk ($\sim 54\text{ Wm}^{-1}\text{K}^{-1}$) [31], as

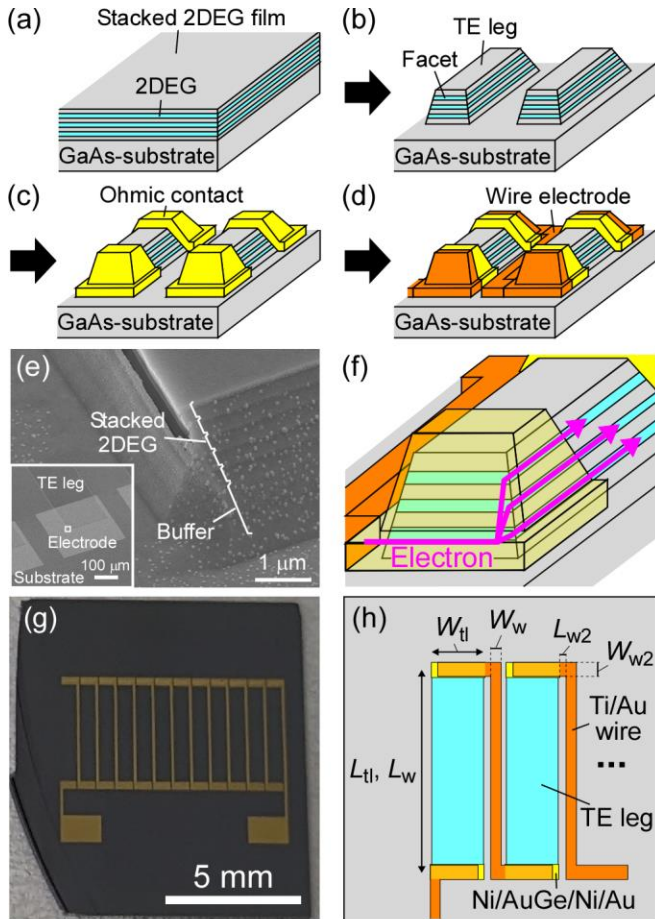


Fig. 3. (a-d) Fabrication processes of stacked 2DEG TEG: (a) Growth of stacked 2DEG film, (b) TE legs by wet etching, (c) Deposition of ohmic electrode, and (d) Deposition of wire electrode. (e) SEM image and (f) schematic illustration of ohmic electrode deposited at the ends of TE legs. (g) Plan-view photograph and (h) schematic illustration of the fabricated stacked 2DEG TEG with $W_{\text{tl}} = 500\text{ }\mu\text{m}$.

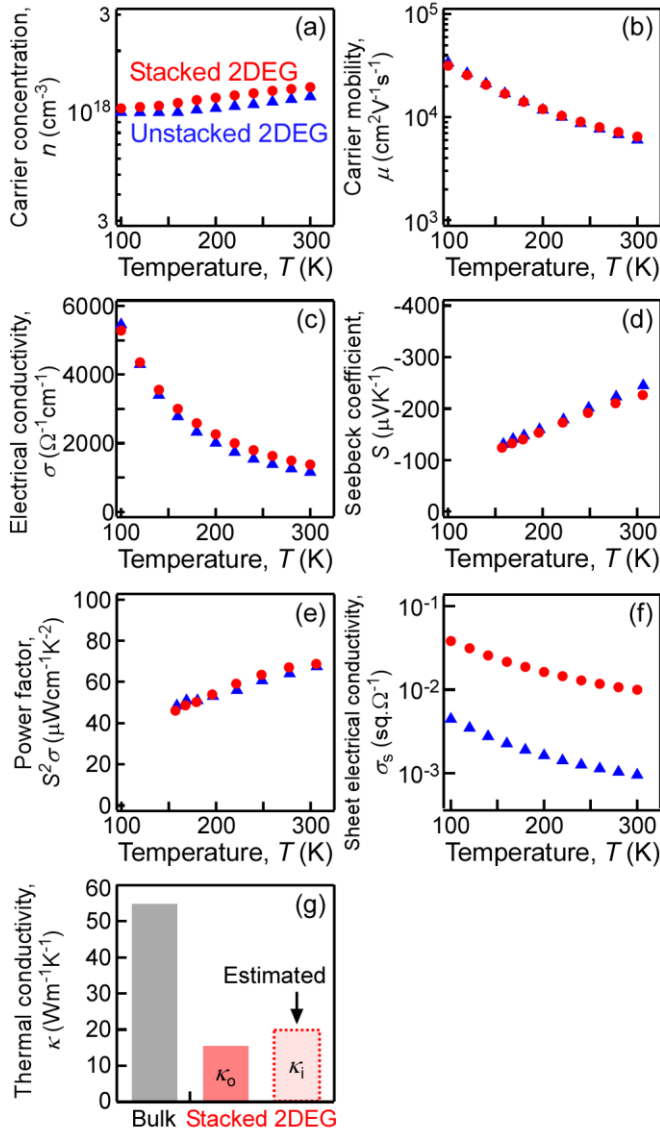


Fig. 4. Temperature dependences of (a) n , (b) μ , (c) σ , (d) S , (e) $S^2\sigma$, (f) σ_s of stacked and unstacked 2DEG films. (g) κ_0 and κ_1 of stacked 2DEG films and κ of GaAs bulk [31].

shown in Fig. 4(g). This κ reduction is likely attributed to the intensified interface phonon scattering in the stacked layer structures of stacked 2DEG films. To estimate the TE performance, it is required to discuss κ and $S^2\sigma$ along the same measurement direction. For this reason, we estimate the in-plane thermal conductivity, κ_1 with reference to the previous results by another group. According to the previous study, the anisotropy rate of κ (κ_1/κ_0) in AlAs/GaAs superlattice was reported to be ~ 1.2 - 1.3 [32]. By using this reported rate, the κ_1 of stacked 2DEG films was estimated to be ~ 20 Wm $^{-1}$ K $^{-1}$. Although the κ_1 of stacked 2DEG films was higher than the κ_0 , the κ_1 of stacked 2DEG films was sufficiently lower than κ of GaAs bulk. This low κ_1 , which is an estimated value, play an important role in applying large ΔT in terms of the thermoelectric devices.

B. Performance of GaAs 2DEG TEGs

Figure 5(a) shows V_{out} and P_{out} of the planar unileg-type stacked GaAs 2DEG film TEG composed of stacked 2DEG films with $W_{tl} = 500$ μ m as a function of I_{out} . During the measurement, the T at the cold side of the TE leg was kept to be 320 K. When increasing ΔT , open-circuit V_{out} V_{oc} and short-circuit I_{out} increased, resulting in the enhancement of the maximum P_{out} , P_{max} . At $\Delta T=4.9$ K, V_{oc} was obtained to be ~ 14 mV, which corresponded to the V_{oc} calculated from the $|S|$ and n_{tl} of the stacked 2DEG film ($|S|=230$ μ VK $^{-1}$, $n_{tl}=12$). This correspondence proves that the applied ΔT was accurately measured and there was no influence of thermal interfacial resistance.

Figure 5(b) summarizes P_{max} values of the three TEGs (stacked 2DEG TEGs with $W_{tl}=500$ μ m and $W_{tl}=200$ μ m, and unstacked 2DEG TEG with $W_{tl}=500$ μ m) as a function of ΔT . We simultaneously plotted the theoretical ΔT - P_{max} curves calculated using the following equations:

$$P_{max} = \frac{(V_{oc})^2}{4R} \quad (1),$$

$$V_{oc} = n_{tl}\Delta T \quad (2),$$

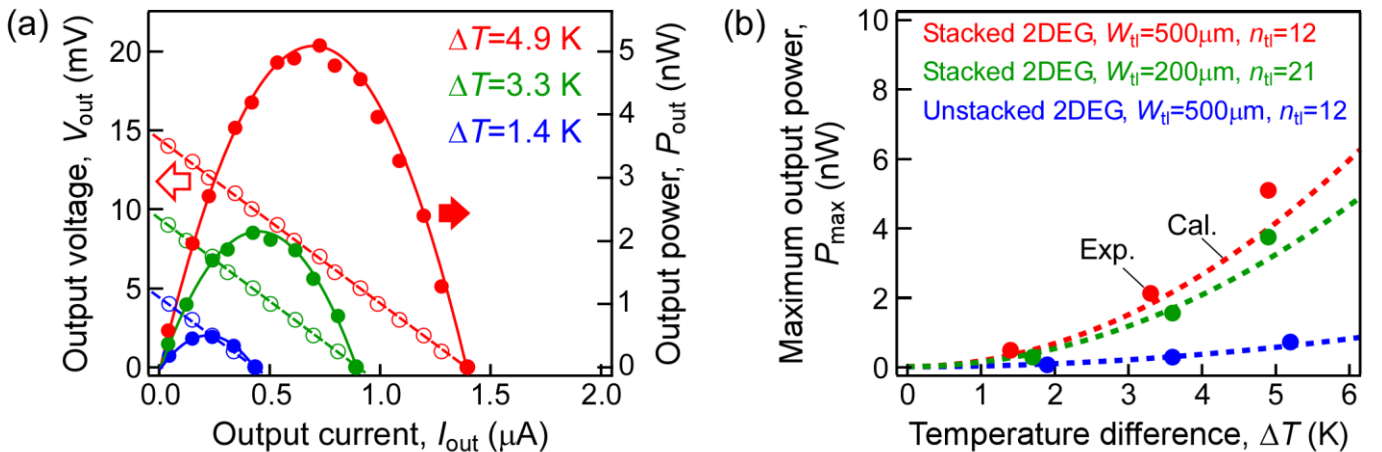


Fig. 5. (a) I_{out} dependences of V_{out} (the open circles) and P_{out} (the solid circles) of the stacked 2DEG TEG with $W_{tl} = 500$ μ m at different temperatures. (b) ΔT dependences of P_{max} of the stacked 2DEG TEGs and the unstacked 2DEG TEG. The broken lines are calculated P_{max} and the solid circles are experimental values of P_{max} .

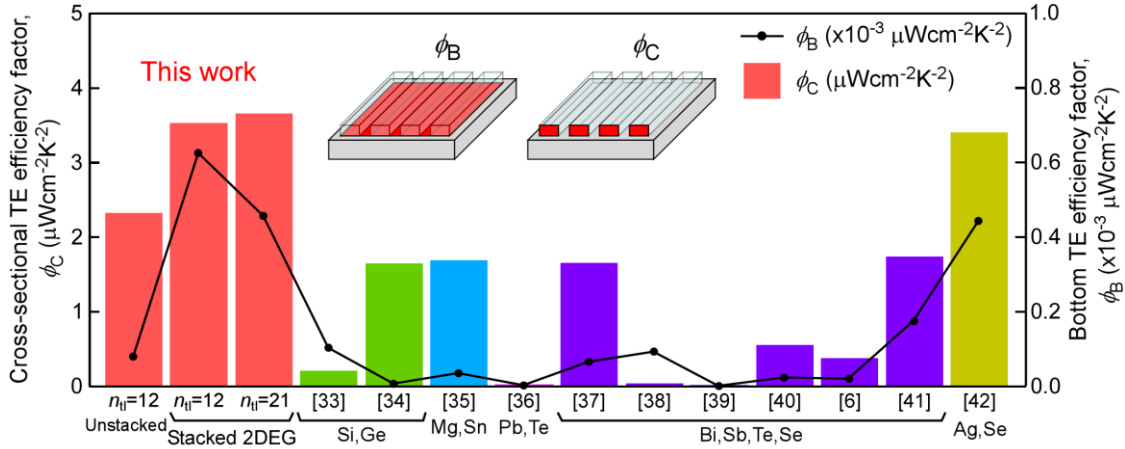


Fig. 6. Comparison of ϕ_B and ϕ_C of our GaAs 2DEG TEGs with other planar type film TEGs without cavities [6], [33]-[42].

$$R = n_{tl} \left(\frac{1}{\sigma_{tl}} \frac{L_{tl} - W_{w2}}{t_{tl} W_{tl}} + \frac{1}{\sigma_{Au}} \left(\frac{L_w - W_{w2}}{t_w W_w} + \frac{2L_{w2} + W_w + W_{tl}}{t_{w2} W_{w2}} \right) \right) \quad (3),$$

where σ_{tl} and σ_{Au} are the electrical conductivity of TE leg and Au electrode. σ_{Au} was experimentally obtained to be $\sim 7 \times 10^3 \Omega^{-1} \text{ cm}^{-1}$ by measuring R of the individual Au wire electrode. Using equation (3) with the designed and the measured parameters, the R values of the TEGs were estimated as follows: 45 k Ω for the stacked 2DEG TEGs with $W_{tl}=200 \mu\text{m}$; 11 k Ω for the stacked 2DEG TEGs with $W_{tl}=500 \mu\text{m}$; 95 k Ω for the unstacked 2DEG TEG.

When increasing ΔT , the experimental P_{\max} values of all the TEGs increased. In all the TEGs, the experimental data agreed well with the theoretical ΔT - P_{\max} curves in the ΔT region of less than 4 K (Fig. 5(b)). On the other hand, there was the slight P_{\max} difference between the experiment and the calculation at the ΔT of ~ 5 K. This could come from the measurement error of the contact resistance or ΔT .

The stacked 2DEG TEGs exhibited ~ 7.5 times higher P_{\max} values than the unstacked 2DEG TEG at almost the same ΔT . This higher P_{\max} is attributed to the lower R of the stacked 2DEG TEGs than that of the unstacked 2DEG TEG. The P_{\max}

of the stacked 2DEG TEGs with $W_{tl}=500 \mu\text{m}$ was higher than that of the stacked 2DEG TEGs with $W_{tl}=200 \mu\text{m}$. From the equations (1)-(3), it is considered that low R and high n_{tl} bring high P_{\max} in the case of the material with the same S . In our experiment, the stacked 2DEG TEG with $W_{tl}=500 \mu\text{m}$ had smaller R of 11 k Ω and n_{tl} of 12 than the stacked 2DEG TEG with $W_{tl}=200 \mu\text{m}$ (R of 45 k Ω and n_{tl} of 21). Namely, in our TEG design, lower R is found to be more effective for enhancing P_{\max} than larger n_{tl} .

In all the TEGs, the experimental P_{\max} values at the ΔT of ~ 5 K were obtained as follows: 3.9 nW for the stacked 2DEG TEGs with $W_{tl}=200 \mu\text{m}$; 5.1 nW for the stacked 2DEG TEGs with $W_{tl}=500 \mu\text{m}$; 0.7 nW for the unstacked 2DEG TEG. We evaluate the TEG performance by comparing the TE efficiency factor ϕ of the planar TEG with those of previous studies without cavities. In the previous studies, ϕ was calculated using two kinds of definition of A : (1) the bottom area of TEG on the substrate and (2) the total cross-sectional area of the TE legs, as shown in Fig. 6. The structures of the planar TEG are shown in Table I. The ϕ values calculated using the bottom area of TEG and the total cross-sectional area were defined as the bottom TE efficiency factor ϕ_B and the cross-sectional TE efficiency factor ϕ_C , respectively. The stacked 2DEG TEGs exhibited higher ϕ_B and ϕ_C than the unstacked 2DEG TEG (Fig. 6). The stacked

TABLE I
STRUCTURES OF THE PLANAR THIN FILM THERMOELECTRIC DEVICES WITHOUT CAVITIES

Reference	p-type	n-type	Thickness of legs	Length of legs	Width of legs	number of legs
This Work	-	Unstacked GaAs 2DEG	0.19 μm	4 mm	0.5 mm	n: 12
This Work	-	Stacked GaAs 2DEG	1 μm	4 mm	0.5 mm	n: 12
This Work	-	Stacked GaAs 2DEG	1 μm	4 mm	0.2 mm	n: 21
[33]	$\text{Si}_{0.8}\text{Ge}_{0.2}$	$\text{Si}_{0.8}\text{Ge}_{0.2}$	10 μm	21.5 mm	3 mm	p: 3, n: 3
[34]	$\text{Si}_{0.85}\text{Ge}_{0.15}$	$\text{Si}_{0.85}\text{Ge}_{0.15}$	0.05 μm	3 mm	2.5 mm	p: 1, n: 2
[35]	$\text{Mg}_2\text{Sn}_{0.8}\text{Ge}_{0.2}$	Bi	0.27 μm	12 mm	0.15 mm	p: 36, n: 36
[36]	$\text{Pb}_{0.925}\text{Yb}_{0.075}\text{Te}$	$\text{Pb}_{0.925}\text{Yb}_{0.075}\text{Se}_{0.2}\text{Te}_{0.8}$	0.95 μm	10 mm	0.4 mm	p: 10, n: 10
[37]	$\text{Bi}_{0.4}\text{Sb}_{1.6}\text{Te}_3$	$\text{Bi}_2\text{Te}_{2.7}\text{Se}_{0.3}$	1 μm	15 mm	1 mm	p: 7, n: 7
[38]	Sb_2Te_3	Bi_2Te_3	30 μm	10 mm	0.3 mm	p: 10, n: 10
[39]	$\text{Bi}_{0.5}\text{Sb}_{1.5}\text{Te}_3$	Bi_2Te_3	0.3 μm	7.8 mm	1 mm	p: 4, n: 4
[40]	$\text{Bi}_{0.5}\text{Sb}_{1.5}\text{Te}_3$	Bi_2Te_3	0.6 μm	15 mm	5 mm	p: 3, n: 3
[6]	$\text{Ag}_{0.005}\text{Bi}_{0.5}\text{Sb}_{1.5}\text{Te}_3$	-	0.75 μm	15 mm	5 mm	p: 4
[41]	$\text{Bi}_{0.5}\text{Sb}_{1.5}\text{Te}_3$	$\text{Bi}_2\text{Te}_{2.4}\text{Se}_{0.6}$	4 μm	20 mm	0.67 mm	p: 15, n: 15
[42]	-	PVP/Ag ₂ Se composite	4.8 μm	20 mm	5 mm	n: 6

2DEG TEGs with $W_{\text{tl}} = 500 \text{ }\mu\text{m}$ and with $W_{\text{tl}} = 200 \text{ }\mu\text{m}$ had the highest ϕ_{B} of $6.3 \times 10^{-4} \text{ }\mu\text{Wcm}^{-2}\text{K}^{-2}$ and the highest ϕ_{C} of $3.7 \text{ }\mu\text{Wcm}^{-2}\text{K}^{-2}$, respectively. Furthermore, the ϕ_{B} and ϕ_{C} values of these stacked 2DEG TEGs were the highest among various simple planar type film TEGs without cavities under the film [6], [33]-[42]. These larger ϕ values and the highly sophisticated fabrication process of GaAs highlight that 2DEG TEG composed of GaAs becomes a promising power source toward the social application.

IV. CONCLUSION

We demonstrated the operation of stacked GaAs 2DEG TEGs composed of M-2DEG films. The stacked GaAs 2DEG exhibited almost the same $S^2\sigma$ as the unstacked GaAs 2DEG. This indicates that 2DEG channels with the same electrical performance are formed even if the triangular well is repeatedly stacked. Thanks to the stacked structure, which intensifies interface phonon scattering, both κ_0 and κ_1 of the stacked GaAs 2DEG were ~ 3 times lower than κ of GaAs bulk. The stacked 2DEG TEGs exhibited 9 times higher σ_s than the unstacked 2DEG TEGs, resulting in ~ 7.5 times higher P_{max} of stacked 2DEG TEGs than that of unstacked 2DEG TEGs. The ϕ_{C} of stacked 2DEG TEGs reached $3.7 \text{ }\mu\text{W cm}^{-2}\text{K}^{-2}$. This ϕ_{C} was the highest among various simple planar type film TEGs without cavities. This study highlights that stacked GaAs 2DEG TEGs become a promising TEG.

REFERENCES

- [1] J. Yan, X. Liao, D. Yan, and Y. Chen, "Review of micro thermoelectric generator," *J. Microelectromech. Syst.*, vol. 27, no. 1, pp. 1-18, Feb. 2018, doi: 10.1109/JMEMS.2017.2782748.
- [2] K. V. Selvan, M. N. Hasan, and M. S. M. Ali, "Methodological reviews and analyses on the emerging research trends and progresses of thermoelectric generators," *Int. J. Energy Res.*, vol. 43, no. 1, pp. 113-140, Sep. 2018, doi: 10.1002/er.4206.
- [3] J. Xie, C. Lee, and H. Feng, "Design, fabrication, and characterization of CMOS MEMS-based thermoelectric power generators," *J. Microelectromech. Syst.*, vol. 19, no. 2, pp. 317-324, Feb. 2010, doi: 10.1109/JMEMS.2010.2041035.
- [4] T. Taniguchi, T. Ishibe, R. Hosoda, Y. Wagatsuma, M. M. Alam, K. Sawano, M. Uenuma, Y. Uraoka, Y. Yamashita, N. Mori, and Y. Nakamura, "Thermoelectric $\text{Si}_{1-x}\text{Ge}_x$ and Ge epitaxial films on Si(001) with controlled composition and strain for group IV element-based thermoelectric generators," *Appl. Phys. Lett.*, vol. 117, no. 14, Oct. 2020, Art. no. 141602, doi: 10.1063/5.0023820.
- [5] S. J. Kim, J. H. We, and B. J. Cho, "A wearable thermoelectric generator fabricated on a glass fabric," *Energy Environ. Sci.*, vol. 7, no. 6, pp. 1959-1965, Mar. 2014, doi: 10.1039/c4ee00242c.
- [6] H. Shang, T. Li, D. Luo, L. Yu, Q. Zou, D. Huang, L. Xiao, H. Gu, Z. Ren, and F. Ding, "High-performance Ag-modified $\text{Bi}_{0.5}\text{Sb}_{1.5}\text{Te}_3$ films for the flexible thermoelectric generator," *ACS Appl. Mater. Interfaces*, vol. 12, no. 6, pp. 7358-7365, Jan. 2020, doi: 10.1021/acsami.9b21771.
- [7] T. Ishibe, A. Tomeda, Y. Komatsubara, R. Kitaura, M. Uenuma, Y. Uraoka, Y. Yamashita, and Y. Nakamura, "Carrier and phonon transport control by domain engineering for high-performance transparent thin film thermoelectric generator," *Appl. Phys. Lett.*, vol. 118, no. 15, Apr. 2021, Art. no. 151601, doi: 10.1063/5.0048577.
- [8] X.-L. Shi, J. Zou, and Z.-G. Chen, "Advanced thermoelectric design: From materials and structures to devices," *Chem. Rev.*, vol. 120, no. 15, pp. 7399-7515, Jul. 2020, doi: 10.1021/acs.chemrev.0c00026.
- [9] T. Cao, X.-L. Shi, and Z.-G. Chen, "Advances in the design and assembly of flexible thermoelectric device," *Prog. Mater. Sci.*, vol. 131, Jan. 2023, Art. no. 101003, doi: 10.1016/j.pmatsci.2022.101003.
- [10] R. Venkatasubramanian, E. Siivola, T. Colpitts, and B. O'Quinn, "Thin-film thermoelectric devices with high room-temperature figures of merit," *Nature*, vol. 413, pp. 597-602, Oct. 2001, doi: 10.1038/35098012.
- [11] A. I. Hochbaum, R. Chen, R. D. Delgado, W. Liang, E. C. Garnett, M. Najarian, A. Majumdar, and P. Yang, "Enhanced thermoelectric performance of rough silicon nanowires," *Nature*, vol. 451, pp. 163-167, Jan. 2008, doi: 10.1038/nature06381.
- [12] Y. Nakamura, M. Isogawa, T. Ueda, S. Yamasaka, H. Matsui, J. Kikkawa, S. Ikeuchi, T. Oyake, T. Hori, J. Shiomi, A. Sakai, "Anomalous reduction of thermal conductivity in coherent nanocrystal architecture for silicon thermoelectric material," *Nano Energy*, vol. 12, pp. 845-851, Mar. 2015, doi: 10.1016/j.nanoen.2014.11.029.
- [13] Y. Nakamura, "Nanostructure design for drastic reduction of thermal conductivity while preserving high electrical conductivity," *Sci. Technol. Adv. Mater.*, vol. 19, no. 1, pp. 31-43, Jan. 2018, doi: 10.1080/14686996.2017.1413918.
- [14] Y. Uematsu, T. Terada, K. Sato, T. Ishibe, and Y. Nakamura, "Low thermal conductivity in single crystalline epitaxial germanane films," *Appl. Phys. Express*, vol. 13, no. 5, Apr. 2020, Art. no. 055503, doi: 10.35848/1882-0786/ab8726.
- [15] T. Taniguchi, T. Terada, Y. Komatsubara, T. Ishibe, K. Konoike, A. Sanada, N. Naruse, Y. Mera, and Y. Nakamura, "Phonon transport in the nano-system of Si and SiGe films with Ge nanodots and approach to ultralow thermal conductivity," *Nanoscale*, vol. 13, no. 9, pp. 4971-4977, Feb. 2021, doi: 10.1039/d0nr08499a.
- [16] T. Ishibe, Y. Komatsubara, K. Ishikawa, S. Takigawa, N. Naruse, Y. Mera, Y. Yamashita, Y. Ohishi and Y. Nakamura, "Boosting thermoelectric performance in epitaxial GeTe film/Si by domain engineering and point defect control" *ACS Appl. Mater. Interfaces*, vol. 15, no. 21, pp. 26104-26110, May 2023, doi: 10.1021/acsami.3c01404.
- [17] Y. Pei, X. Shi, A. LaLonde, H. Wang, L. Chen, and G. J. Snyder, "Convergence of electronic bands for high performance bulk thermoelectrics," *Nature*, vol. 473, pp. 66-69, May 2011, doi: 10.1038/nature09996.
- [18] A. Samarelli, L. F. Llin, S. Cecchi, J. Frigerio, T. Etzelstorfer, E. Müller, Y. Zhang, J. R. Watling, D. Chrastina, G. Isella, J. Stangl, J. P. Hague, J. M. R. Weaver, P. Dobson, and D. J. Paul, "The thermoelectric properties of Ge/SiGe modulation doped superlattices," *J. Appl. Phys.*, vol. 113, no. 23, Jun. 2013, Art. no. 233704, doi: 10.1063/1.4811228.

- [19] G. Tan, F. Shi, S. Hao, H. Chi, L.-D. Zhao, C. Uher, C. Wolverton, V. P. Dravid, and M. G. Kanatzidis, "Codoping in SnTe: enhancement of thermoelectric performance through synergy of resonance levels and band convergence," *J. Am. Chem. Soc.*, vol. 137, no. 15, pp. 5100-5112, Apr. 2015, doi: 10.1021/jacs.5b00837.
- [20] T. Ishibe, A. Tomeda, K. Watanabe, Y. Kamakura, N. Mori, N. Naruse, Y. Mera, Y. Yamashita, and Y. Nakamura, "Methodology of thermoelectric power factor enhancement by controlling nanowire interface," *ACS Appl. Mater. Interfaces*, vol. 10, no. 43, pp. 37709-37716, Oct. 2018, doi: 10.1021/acsami.8b13528.
- [21] S. Sakane, T. Ishibe, K. Mizuta, T. Fujita, Y. Kiyofuji, J. Ohe, E. Kobayashi, and Y. Nakamura, "Anomalous enhancement of thermoelectric power factor by thermal management with resonant level effect," *J. Mater. Chem. A*, vol. 9, no. 8, pp. 4851-4857, Jan. 2021, doi: 10.1039/d0ta08683e.
- [22] T. Terada, Y. Uematsu, T. Ishibe, N. Naruse, K. Sato, T. Q. Nguyen, E. Kobayashi, H. Nakano, and Y. Nakamura, "Giant enhancement of Seebeck coefficient by deformation of silicene buckled structure in calcium-intercalated layered silicene film," *Adv. Mater. Interfaces*, vol. 9, no. 1, Jan. 2022, Art. no. 2101752, doi: 10.1002/admi.202101752.
- [23] L. D. Hicks and M. S. Dresselhaus, "Effect of quantum-well structures on the thermoelectric figure of merit," *Phys. Rev. B*, vol. 47, no. 19, pp. 12727-12731, May 1993, doi: 10.1103/PhysRevB.47.12727.
- [24] H. Ohta, S.W. Kim, Y. Mune, T. Mizoguchi, K. Nomura, S. Ohta, T. Nomura, Y. Nakanishi, Y. Ikuhara, M. Hirano, H. Hosono, and K. Koumoto, "Giant thermoelectric Seebeck coefficient of a two-dimensional electron gas in SrTiO₃," *Nat. Mater.*, vol. 6, pp. 129-134, Jan. 2007, doi: 10.1038/nmat1821.
- [25] Y. Zhang, B. Feng, H. Hayashi, C.-P. Chang, Y.-M. Sheu, I. Tanaka, Y. Ikuhara, and H. Ohta, "Double thermoelectric power factor of a 2D electron system," *Nat. Commun.*, vol. 9, Jun. 2018, Art. no. 2224, doi: 10.1038/s41467-018-04660-4.
- [26] N. T. Hung, E. H. Hasdeo, A. R. T. Nugraha, M. S. Dresselhaus, and R. Saito, "Quantum effects in the thermoelectric power factor of low-dimensional semiconductors," *Phys. Rev. Lett.*, vol. 117, Jul. 2016, Art. no. 036602, doi: 10.1103/PhysRevLett.117.036602.
- [27] H. Ohta, S. W. Kim, S. Kaneki, A. Yamamoto, and T. Hashizume, "High thermoelectric power factor of high-mobility 2D electron gas," *Adv. Sci.*, vol. 5, no. 1, Jan. 2018, Art. no. 1700696, doi: 10.1002/advs.201700696.
- [28] Y. Uematsu, T. Ishibe, T. Mano, A. Ohtake, H. T. Miyazaki, T. Kasaya, and Y. Nakamura, "Anomalous enhancement of thermoelectric power factor in multiple two-dimensional electron gas system," *Nat. Commun.*, vol. 15, Jan. 2024, Art. no. 322, doi: 10.1038/s41467-023-44165-3.
- [29] I.-H. Tan, G. L. Snider, L. D. Chang, and E. L. Hu, "A self-consistent solution of Schrödinger-Poisson equations using a nonuniform mesh," *J. Appl. Phys.*, vol. 68, no. 8, pp. 4071-4076, Oct. 1990, doi: 10.1063/1.346245.
- [30] L. Pfeiffer, K. W. West, H. L. Stormer, and K. W. Baldwin, "Electron mobilities exceeding 10^7 cm²/V s in modulation-doped GaAs," *Appl. Phys. Lett.*, vol. 55, no. 18, pp. 1888-1890, Oct. 1989, doi: 10.1063/1.102162.
- [31] R. O. Carlson, G. A. Slack, and S. J. Silverman, "Thermal conductivity of GaAs and GaAs_{1-x}P_x laser semiconductors," *J. Appl. Phys.*, vol. 36, no. 2, pp. 505-507, Jul. 1965, doi: 10.1063/1.1714018.
- [32] M. N. Luckyanova, J. A. Johnson, A. A. Maznev, J. Garg, A. Jandl, M. T. Bulsara, E. A. Fitzgerald, K. A. Nelson, and G. Chen, "Anisotropy of the thermal conductivity in GaAs/AlAs superlattices," *Nano Lett.*, vol. 13, no. 9, pp. 3973-3977, Aug. 2013, doi: 10.1021/nl4001162.
- [33] K. Xie and M. C. Gupta, "High-temperature thermoelectric energy conversion devices using Si-Ge thick films prepared by laser sintering of nano/micro particles," *IEEE Trans. Electron. Devices*, vol. 67, no. 5, pp. 2113-2119, Mar. 2020, doi: 10.1109/TED.2020.2977832.
- [34] M. Tsujii, M. Murata, A. Yamamoto, T. Suemasu, and K. Toko, "Thin-film thermoelectric generator based on polycrystalline SiGe formed by Ag-induced layer exchange," *Appl. Phys. Lett.*, vol. 117, no. 16, Oct. 2020, Art. no. 162103, doi: 10.1063/5.0021880.
- [35] I. Ohkubo, M. Murata, M. S.L. Lima, T. Sakurai, Y. Sugai, A. Ohi, T. Aizawa, and T. Mori, "Miniaturized in-plane π -type thermoelectric device composed of a II-IV semiconductor thin film prepared by microfabrication," *Mater. Today Energy*, vol. 28, Aug. 2022, Art. no. 101075, doi: 10.1016/j.mtener.2022.101075.
- [36] A. Hmood, A. Kadhim, J. J. Hassan, and H.A. Hassan, "Thermoelectric generators using p-Pb_{0.925}Yb_{0.075}Te:Te and n-Pb_{0.925}Yb_{0.075}Se_{0.2}Te_{0.8} thin films prepared by the thermal evaporation method," *J. Electron. Mater.*, vol. 42, pp. 1146-1153, Apr. 2013, doi: 10.1007/s11664-013-2542-y.
- [37] M. Takashiri, T. Shirakawa, K. Miyazaki, and H. Tsukamoto, "Fabrication and characterization of bismuth-telluride-based alloy thin film thermoelectric generators by flash evaporation method," *Sens. Actuators A*, vol. 138, no. 2, pp. 329-334, Aug. 2007, doi: 10.1016/j.sna.2007.05.030.
- [38] M. Mizoshiri, M. Mikami, K. Ozaki, M. Shikida, and S. Hata, "Lift-off patterning of thermoelectric thick films deposited by a thermally assisted sputtering method," *Appl. Phys. Express*, vol. 7, no. 5, Apr. 2014, Art. no. 057101, doi: 10.7567/APEX.7.057101.
- [39] N.-W. Park, T.-H. Park, J.-Y. Ahn, S.-H. Kang, W.-Y. Lee, Y.-G. Yoon, S.-G. Yoon, and S.-K. Lee, "Thermoelectric characterization and fabrication of nanostructured p-type Bi_{0.5}Sb_{1.5}Te₃ and n-type Bi₂Te₃ thin film thermoelectric energy generator with an in-plane planar structure," *AIP Adv.*, vol. 6, no. 6, Jun. 2016, Art. no. 065123, doi: 10.1063/1.4955000.
- [40] H. Shang, C. Dun, Y. Deng, T. Li, Z. Gao, L. Xiao, H. Gu, D. J. Singh, Z. Ren, and F. Ding, "Bi_{0.5}Sb_{1.5}Te₃-based films for flexible thermoelectric devices," *J. Mater. Chem. A*, vol. 8, no. 8, pp. 4552-4561, Feb. 2020, doi: 10.1039/c9ta13152c.
- [41] I.-H. Kim, "(Bi,Sb)₂(Te,Se)₃-based thin film thermoelectric generators," *Mater. Lett.*, vol. 43, no. 5-6, pp. 221-224, May 2000, doi: 10.1016/S0167-577X(99)00239-6.
- [42] C. Jiang, P. Wei, Y. Ding, K. Cai, L. Tong, Q. Gao, Y. Lu, W. Zhao, and S. Chen, "Ultrahigh performance polyvinylpyrrolidone/Ag₂Se composite thermoelectric film for flexible energy harvesting," *Nano Energy*, vol. 80, Feb. 2021, Art. no. 105488, doi: 10.1016/j.nanoen.2020.105488.